Biosensors and Bioelectronics 227 (2023) 115097

Contents lists available at ScienceDirect

Biosensors and Bioelectronics

journal homepage: www.elsevier.com/locate/bios

A non-invasive wearable stress patch for real-time cortisol monitoring using a pseudoknot-assisted aptamer

Naveen K. Singh [a,1], Saeromi Chung [a,1], An-Yi Chang [b], Joseph Wang [b], Drew A. Hall [a,c,*]

[a] Department of Electrical and Computer Engineering, University of California – San Diego, La Jolla, CA, 92093, USA
[b] Department of Nanoengineering, University of California – San Diego, La Jolla, CA, 92093, USA
[c] Department of Bioengineering, University of California – San Diego, La Jolla, CA, 92093, USA

ARTICLE INFO

Keywords:
Electrochemical aptasensor
Pseudoknot aptamer
Cortisol
Sweat monitoring
Wearable sensor
Microfluidic

ABSTRACT

Stress is part of everyone's life and is exacerbated by traumatic events such as pandemics, disasters, violence, lifestyle changes, and health disorders. Chronic stress has many detrimental health effects and can even be life-threatening. Long-term stress monitoring outside of a hospital is often accomplished by measuring heart rate variability. While easy to measure, this digital biomarker has low specificity, greatly limiting its utility. To address this shortcoming, we report a non-invasive, wearable biomolecular sensor to monitor cortisol levels in sweat. Cortisol is a neuroendocrine hormone that regulates homeostasis as part of the stress pathway. Cortisol is detected using an electrochemical sensor functionalized with a pseudoknot-assisted aptamer and a flexible microfluidic sweat sampling system. The skin-worn microfluidic sampler provides rapid sweat collection while separating old and new sweat. The conformation-switching aptamer provides high specificity towards cortisol while being regenerable, allowing it to monitor temporal changes continuously. The aptamer was engineered to add a pseudoknot, restricting it to only two states, thus minimizing the background signal and enabling high sensitivity. An electrochemical pH sensor allows pH-corrected amperometric measurements. Device operation was demonstrated *in vitro* with a broad linear dynamic range (1 pM - 1 μM) covering the physiological range and a sub-picomolar (0.2 pM) limit of detection in sweat. Real-time, on-body measurements were collected from human subjects using an induced stress protocol, demonstrating *in-situ* signal regeneration and the ability to detect dynamic cortisol fluctuations continuously for up to 90 min. The reported device has the potential to improve prognosis and enable personalized treatments.

1. Introduction

Wearable sensors have drawn significant attention recently for healthcare (Windmiller and Wang, 2013; huber, 2016; Zeng et al., 2022), fitness (M. Wang et al., 2022), risk mitigation (Mahmud et al., 2018), rehabilitation (Patel et al., 2012), and environmental applications (Gao et al., 2016; Parlak et al., 2018; Xu et al., 2014). Healthcare- and fitness-focused wearable sensors enable continuous monitoring, allowing individuals to track key vitals, metabolite levels, and other important biosignals (*e.g.*, infection, inflammation) in real-time to support proactive healthcare and wellness. Integrating these wearable sensors with smart devices (*e.g.*, smartphones, smartwatches) also permits healthcare providers to detect sudden fluctuations or baseline changes of target biomarkers and supports earlier intervention with better and more effective predictive and theragnostic opportunities (Sanjay et al., 2020). Over the last decade, many wearable sensors have been commercialized with heart rate (HR), respiratory rate (RR), and pulse oxygenation (SpO_2) monitoring, making such devices nearly ubiquitous today. Except for continuous glucose monitors (CGMs), there has been much less progress in sensing biomolecular signals, and the ability to detect stress levels is a long-sought-after goal (Samson and Koh, 2020). Current stress monitoring wearables indirectly measure the individual's stress level through heart rate variability (HRV) – a derived metric that works best when a person is at rest; however, the utility is diminished when in movement (Etiwy et al., 2019). Furthermore, these sensors fundamentally lack specificity as they measure a downstream effect (*i.e.,* HRV) rather than the originating biomolecular signal (*e.g.*, the release of cortisol). Thus, research is moving toward non-invasive

* Corresponding author. Department of Electrical and Computer Engineering, University of California – San Diego, La Jolla, CA, 92093, USA.
E-mail address: drewhall@ucsd.edu (D.A. Hall).
[1] Equally credited authors.

https://doi.org/10.1016/j.bios.2023.115097
Received 2 December 2022; Received in revised form 29 December 2022; Accepted 19 January 2023
Available online 29 January 2023

wearable chemical sensors that monitor clinically relevant biomarkers from easily accessible biofluids such as sweat, interstitial fluid, tears, and saliva (Bandodkar et al., 2016; Kim et al., 2016; Oncescu et al., 2013; Sempionatto et al., 2017; Singh et al., 2019).

Stress is a biological response evoked by any stimulus that causes physio-psychological strain. It can initiate numerous bodily actions, from stress axis dysfunction (hypothalamic pituitary adrenal axis) and change in homeostasis to life-threatening effects and even death (Chrousos, 2009). Cortisol is released into the bloodstream by the adrenal gland in response to emotional and/or psychological stress and distributed throughout the body in several biofluids. Cortisol is an important neuroendocrine hormone responsible for maintaining homeostasis by regulating immune, neurochemical, metabolic, and cardiovascular functions in response to stress. The cortisol level in biofluids follows the circadian rhythm throughout the day, with the highest level in the morning and the lowest at night. Moreover, cortisol levels fluctuate throughout the day per exposure to various psychological and physiological stressors (Sakihara et al., 2010). Importantly, cortisol is present in sweat (7.9–141 ng/mL) and changes rapidly according to a person's stress level (Katchman et al., 2018; Kinnamon et al., 2017; Singh et al., 2021a). Thus, there is a need for a continuous monitoring system that can determine dynamic cortisol levels under stress-provoking conditions without needing a cumbersome laboratory setup.

Sweat is a convenient biofluid for non-invasive wearable sensors because it has abundant biochemical information with a simple sample collection (Brasier and Eckstein, 2019; Katchman et al., 2018; Kinnamon et al., 2017; Kintz et al., 1996). The normal perspiration rate from human skin is ~2 μL/min/cm^2 and can be increased on demand through electrical or chemical stimulation (Katchman et al., 2018). Locating the sensor at the generation site facilitates rapid analysis before the analytes degrade (Fig. 1). These advantages have led to a wide range of epidermal sensing devices to monitor metabolites and electrolytes (Ghaffari et al., 2021; Kinnamon et al., 2017). However, several key challenges, such as the low secretion rate, variability, evaporation, amalgamation, and separation of old and new sweat, must be addressed to achieve accurate, consistent real-time measurements (Ghaffari et al., 2021). Moreover, due to the complex nature of the perspiration and reabsorption mechanism, sweat composition, pH, biomarker concentration, and sweat secretion rate are indistinguishably linked (Dang et al., 2018; De Giovanni and Fucci, 2013; Heikenfeld, 2016; Herrmann and Mandol, 1955). Addressing these challenges is vital to realizing the full potential of sweat-based sensors.

Microfluidics has long been used for *in vitro* applications to manipulate small fluid volumes, and their integration with wearable sweat sensors can overcome several of the aforementioned challenges. Specifically, microfluidics allow rapid sweat transport and minimize the mixing and carry-over effect of old and new sweat with a well-defined encapsulated sensing chamber. This also separates the sensing and sweat generation/collection region to minimize contamination and evaporation while enhancing the sensitivity (Nyein et al., 2018; Vinoth et al., 2021). Only a few wearable microfluidic-based sweat sensors have been reported, and they have short lifetimes (<1 h), precluding the vision of a long-term monitoring system (Anastasova et al., 2017; Koh et al., 2016; Martín et al., 2017; Xu et al., 2014).

Various probes can be used to capture and detect cortisol; however, aptamers have emerged as a leading candidate for detecting targets in complex biofluids in recent years due to their advantages over other probes, such as antibodies, enzymes, and molecular imprinted polymers (MIP) (Singh et al., 2021b, 2021c, 2019). Aptamer-based assays require

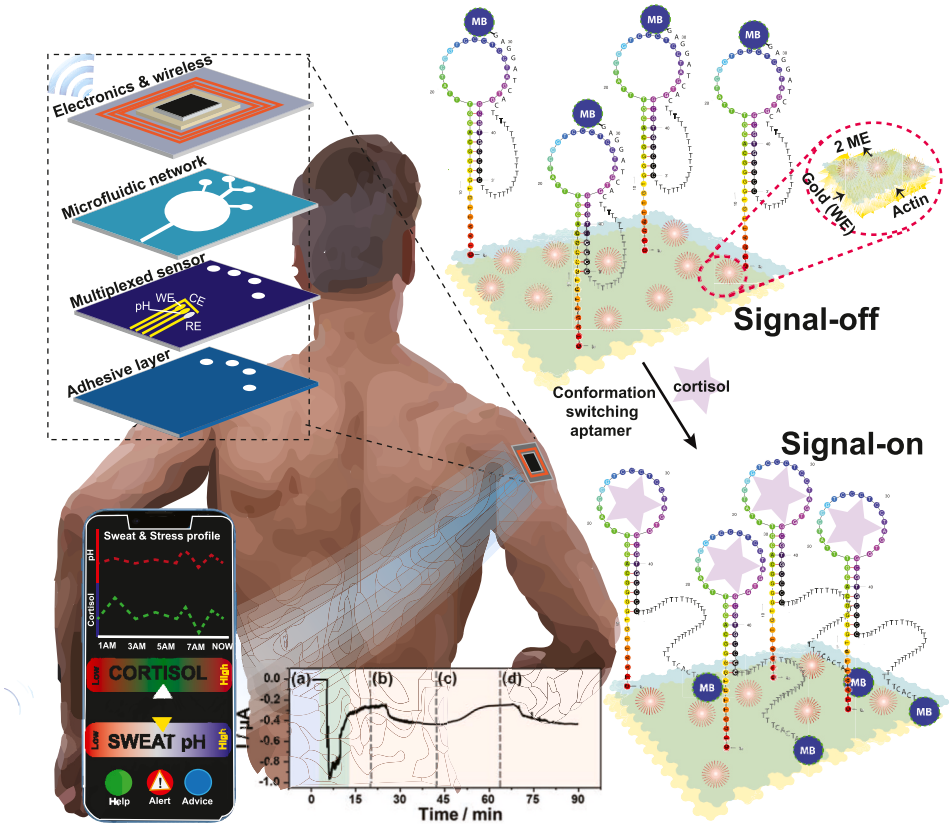

Fig. 1. Illustration of wearable sweat patch for monitoring cortisol levels. The microfluidic-coupled electrochemical sensor captures, proceesses, and detects cortisol levels in real-time using a conformation-switching aptamer with a pseudoknot structure. The cortisol concentration and sweat pH measurements can be transferred wirelessly for display and analysis on a nearby smart device.

minimal reagents (Chung et al., 2021), washing steps (Chen et al., 2020) and enable sensor regeneration for real-time reversible measurements (Ferguson et al., 2013; Plaxco and Soh, 2011; Schoukroun-Barnes et al., 2016). Many electrochemical aptamer-based sensors with target-dependent conformation-switching have been reported (Ferguson et al., 2013; Plaxco and Soh, 2011). Although these sensors allow convenient biomarker detection, the sensitivity is compromised by the high background current and low transduction efficiency (Chen et al., 2020; Chung et al., 2021; Singh et al., 2021a). In particular, the background current in conformation-switching aptamer assays is relatively high because the signaling molecule's position in the unbound state is not well defined, unlike the bound state. Applying semirigid DNA structures, such as a double hairpin, allows pseudoknot-like aptamer structures to overcome this limitation by restricting the aptamer to two well-defined states (Jiang et al., 2015). Since aptamer binding affinity and electrochemical properties of redox labels (*e.g.,* methylene blue, ferrocene, and ruthenium) vary in a pH-dependent manner, accurate target concentration estimation is challenging in biofluids such as sweat, urine, and saliva (Belleperche and DeRosa, 2018; Drolen et al., 2018; Gordon et al., 2018; Ju et al., 1995).

We report a wearable patch based on soft microfluidics and flexible electrodes functionalized with a pseudoknot-assisted conformation-switching aptamer for pH-calibrated, continuous, non-invasive cortisol monitoring in sweat, as shown in Fig. 1. The gold electrodes are sputtered on a flexible polydimethylsiloxane (PDMS) substrate consisting of two working electrodes (pH and probe), a counter electrode, and an Ag/AgCl reference electrode. The electrodes are sandwiched between two thin PDMS layers adhered with double-sided tape. One layer has the electrodes, while the other contains the detection reservoir and microfluidic channels. The patch provides skin-adherable sampling, fluidics, and detection in a unified device, ensuring efficient sweat transport over the detector surface while addressing skin contamination and sweat carry-over issues. A conformation-switching cortisol aptamer was engineered with a methylene blue (MB) redox reporter on the distal end and short complementary regions interspaced with poly-thymine (T-12) spacers to realize a pseudoknot structure. When cortisol binds to the aptamer, the conformation switches from the pseudoknot form to a one-stem-loop structure, displacing the stem at the 3′-terminus and enhancing the electron transfer rate due to the close proximity between the redox tag and electrode surface. This leads to a change in current proportional to the cortisol concentration. The resulting wearable electrochemical sensor exhibited a broad dynamic range (1 pM - 10 μM) with a sub-picomolar limit of detection in sweat. The patch was validated by measuring cortisol in real-time on three human subjects with induced stress. Such a skin-conforming microfluidic aptamer-based chemical sensing system has great potential to help individuals maintain optimal health and evaluate their physiological and psychological wellness.

2. Materials and methods

2.1. Reagents and instruments

The 5′-modified HPLC-grade purified aptamer for cortisol (Yang et al., 2017) was ordered from Integrated DNA Technology (IDT), USA. Semirigid structures were engineered and added to form the pseudoknot. The aptamer sequences with their respective modifications are reported in Table 1, where *N* denotes the overlap length for the semirigid structure. Cortisol, IgG (immunoglobulin G), C reactive protein (CRP), epinephrine, and actin were procured from Sigma. Various salts, bovine serum albumin (BSA), and glucose (#A16828) were obtained from Thermo Fisher. Dulbecco potassium phosphate buffer (PBS; #P5493), Iron (III) chloride ($FeCl_3$), polyaniline salt, Nafion solution, 2-mercaptoethanol (2 ME; #M6250), sulfuric acid (H_2SO_4; #339741), Tris[2-carboxyethyl] phosphine (TCEP; #C4706), magnesium chloride ($MgCl_2$; #208337), calcium chloride ($CaCl_2$; #C5670), phosphate-buffered saline nuclease-free water (#3098), ascorbic acid (AA; #A5960), (3-mercaptoprolyl)triethoxysilane (#63797), and methylene blue (MB) were purchased from Sigma Aldrich. Amicon 10 kDa cutoff filters were purchased from Millipore. Sylgard 184 silicone elastomer kit (#24236–10) was purchased from Electron Microscopy Sciences (USA, PA). The buffer compositions used in this work are described in Supplemental Table S1. All reagents were of analytical grade and used without any further processing.

Screen-printed electrodes (SPEs; #AT220) with a gold working electrode (WE), gold counter electrode (CE), and a silver reference electrode (RE) were purchased from Metrohm. The thin-film gold electrodes were created by sputtering gold on PDMS. Electrochemical impedance spectroscopy (EIS), cyclic voltammetry (CV), differential pulse voltammetry (DPV), and chronoamperometry (CA) measurements were performed using a PalmSens4 potentiostat (PalmSens BV, The Netherlands).

2.2. Microfluidic channel design and fabrication

The microfluidic channel and 3D printed mold to fabricate the PDMS-based microfluidics were designed using AutoCAD and 3ds Max. The PDMS is 500 μm thick with four inlets (300 μm height), a reservoir (0.5 cm radius), and one outlet. The 3D mold with a micro-structured surface was printed using a Form 3 3D printer (Formlabs, USA) with v4 resin. The printed mold was washed with isopropyl alcohol (IPA) for 20 min and ultraviolet (UV) cured to polymerize the resin for 60 min at 60 °C. A sacrificial poly methyl methacrylate (PMMA) layer was then coated on the mold surface and cured at 80 °C to dry the volatile solvents. The PDMS (Dow Corning, Sylgard 184) was degassed and mixed with the curing agent (15:1 ratio) at 25 in Hg. The PDMS mixture was poured into the mold and then polymerized by soft baking for 2 h at 80 °C in a vacuum oven. The PDMS/PMMA/mold was then sonicated for 10 min in IPA, and the separated PDMS/PMMA layer was incubated in 50 °C acetone for 1 h and IPA overnight to remove the PMMA.

2.3. Simulation of sweat fluid dynamics

Fluid dynamics simulations of the microfluidics were carried out using COMSOL Multiphysics. The sweat flow rate and pressure were simulated to verify the fluid behavior under sweat sampling conditions. Simulations were done using water since sweat is 99% water with a sweat rate of 32.5 nL/min/gland. For the simulation, 7.7 glands were used based on the opening area of the microfluidic channel and sweat gland density of human skin. The fluidic design was drawn to scale, and PDMS was selected as the material.

Table 1
Aptamer sequences; pseudoknot forming region in bold and linker region in italics.

Cortisol aptamer	Sequences (5' -> 3')
w/o pseudoknot	Thiol-CTCTCGGGACGACGCCAGAAGTTTACGAGGATATGGTAACATAGTCGTCCC-MB
Pseudoknot N5	Thiol-CTCTCGGGACGACGCCAGAAGTTTACGAGGATATGGTAACATAGTCGTCCC*TTTTTTTTTTT***GGTCT** -MB
Pseudoknot N8	Thiol-CTCTCGGGACGACGCCAGAAGTTTACGAGGATATGGTAACATAGTCGTCCC*TTTTTTTTTTT***GGTCT TCA**-MB
Pseudoknot N11	Thiol-CTCTCGGGACGACGCCAGAAGTTTACGAGGATATGGTAACATAGTCGTCCC*TTTTTTTTTTT***GGTCT TCAAAT**-MB
Pseudoknot N14	Thiol-CTCTCGGGACGACGCCAGAAGTTTACGAGGATATGGTAACATAGTCGTCCC*TTTTTTTTTTT***GGTCT TCAAATGCT**-MB

2.4. Electrode design and fabrication

The wearable electrochemical sensor consisting of two WEs, a RE, and a CE with a 1.5 mm pitch was drawn using AutoCAD (Supplemental Fig. S1). A silicon wafer (500 μm thickness, 10 cm diameter) was placed on the PMMA-treated circular 3D printed mold (12 cm outer diameter, 10 cm inner diameter, 1 mm thickness) to fabricate the PDMS substrate for the electrodes. PDMS was poured onto the wafer/mold and degassed under 25 in Hg vacuum for 20 min. The PDMS was polymerized at 80 °C in a vacuum oven for 2 h and separated from the mold by immersing it in acetone. The PDMS was then washed with IPA and UV-ozone treated for 10 min. Finally, the PDMS was silanized with (3-Mercaptopropyl)trimethoxysilane for Au deposition.

Two layers of polyimide high-temperature resistant tape (purchased from Amazon) were placed on transparent flexible PET sheets (134 μm thick) without air bubbles and fixed on a cutting mat with blue tape. The mask was designed using Cricut Design Space (v7.10.163) and uploaded to the Cricut Explore Air® 2 with a 60° deep cut blade. Following the mask fabrication, the double-layer tape with the mask design was gently removed from the polyethylene terephthalate (PET) sheet using transfer tape, placed on the top of the prepared thin PDMS form, and then kept in the single wafer sample box. Before sputtering, the PDMS with mask design tape was cleaned with a nitrogen spray gun. Subsequently, the samples were fixed on the sputtering sample stage with tape and sputtered with chromium (Cr) and gold (Au) using a Denton Discovery 635 Sputter System (Denton Vacuum, USA). The Cr was sputtered at 300 W dc power for 6 min, and Au was sputtered on top of Cr at 100 W dc power for 15 min. All sputtering was carried out at 65% rotation and 2.51 mTorr chamber pressure with Ar gas in a class 100 cleanroom.

2.5. Electrode cleaning and sensor fabrication

Before modifying the sensor, the electrodes were cleaned in ethanol by sonication for 5 min, followed by electrochemical cleaning in 0.1 M H_2SO_4 by potential cycling from 0 to +1.5 V (15 cycles) at a 100 mV/s scan rate to remove organic residues and contamination on the electrode surface. The electrode was then thoroughly washed with distilled water and air-dried. Before functionalizing the electrode with the aptamer (10 μM), it was mixed with TCEP (100 μM) in water and incubated for 1 h at room temperature. Then the mixture was diluted with binding buffer to the final concentration. Next, 10 μL of the mixture was drop-casted on the working electrode. The complex was incubated overnight in a humidity chamber at 4 °C, followed by rinsing with binding buffer to remove unbound/loosely bound aptamers from the sensor surface. The unoccupied exposed gold surface was blocked by incubating 1 mM 2-mercaptoethanol (2 ME) for 30 min, followed by washing with ultrapure water. To ensure proper coverage and prevent non-specific adsorption, the electrodes were further blocked with a 2 μM actin protein solution for 30 min. The electrode was again washed with ultrapure water and air-dried. The pH sensor was fabricated by drop-casting 1 mg/mL polyaniline (PANI) and 0.5% Nafion in ethanol over the gold electrode. The electrode was dried at room temperature for 1 h. The pH sensor was washed with ultrapure water and stored at 4 °C. The modified Au electrodes on PDMS were assembled with UV-Ozone-treated microfluidics using the PDMS as a glue (Wu et al., 2005). Following assembly, the devices were cured at 60 °C for 90 min and then stored at 4 °C for later use.

2.6. in vitro electrochemical measurement

The cortisol sensors were incubated with cortisol spiked in binding buffer or artificial sweat for 5 min, and a DPV voltammogram was recorded. The cortisol measurement was also performed under the flow injection using the microfluidics. The fabricated sensor was placed inside the sample holding region of the microfluidic device, and buffer or artificial sweat was pumped with a syringe infusion pump at 20 μL/min to mimic the sweat rate of a healthy individual. Varying concentrations of cortisol solution were tested. DPV measurements were performed from −0.6 V to 0.0 V (vs. Ag/AgCl) with a 70-mV step and 20 s duration at a scan rate of 50 mV/s. The pH sensor was characterized by measuring the open circuit potential (OCP) in buffer with different pH solutions. Buffer solution was placed over the electrode, and OCP readings were carried out for 5 min.

2.7. On-body measurements with human subjects

On-body sensor testing with human subjects was performed following a protocol approved by the institutional review board (IRB #130003-epidermal) at the University of California, San Diego. The sensor was tested for 1) sweat collection and 2) cortisol detection. The microfluidic device was attached to the skin using double-sided medical tape with 2 mm openings connected with the inlets of the device. The device was mounted on the back of the subject's lower neck as a tradeoff between the optimum sweat rate, lack of body hair, minimal movement, and ease of connection to the external potentiostat. For the sweat collection test, bare Au electrodes were used to evaluate the sensor's collection ability. We first dropped blue food coloring dye (0.5 μL) on the sweat collection area. After attaching the microfluidic device to the volunteer's skin, the volunteer exercised using a stationary bike under ambient conditions. For cortisol detection, we connected the microfluidic devices to a portable potentiostat.

2.8. Statistical analysis

The data presented are the mean of three independent experiments performed with independently fabricated devices under similar conditions, while the error bars represent one standard deviation. Statistical analysis was performed with Origin (v9.0). The limit of detection (LOD) was calculated using 3 × the standard deviation of the y-intercept/slope (Brunetti B, 2015).

3. Results and discussion

The two-state structure of the pseudoknot-assisted aptamer on a microfluidic-enabled wearable sensor for cortisol monitoring in real-time from sweat is illustrated in Fig. 1. The original aptamer (Yang et al., 2017), containing one loop and two stem regions, was extended with a complementary region with poly T (T_{12}) oligonucleotides to the stem region to facilitate hybridization with the loop structure. This designed complementary region assists in the formation of a stable pseudoknot structure. However, there is a tradeoff in the added complementary region – too short, and it is not stable, yet too long, and the structure loses affinity to the target. As illustrated in Supplemental Fig. S2, the aptamer binding structure is conserved among pseudoknot aptamers of various lengths (N5 to N14). The 5' end of the aptamer was immobilized on the gold electrode through gold-thiol bond formation, while the 3' was labeled with a redox tag (methylene blue) for signaling. When cortisol binds with the aptamer, it undergoes conformation switching, bringing the 3' attached redox tag close to the surface and enhancing the current response (Fig. 2A). In the absence of cortisol, the designed probe remains in the pseudoknot form, and the redox tag is far from the sensor surface. Notably, this reduces the background current as the redox tag is modulated between two well-defined positions, unlike most conformation-switching aptamers with only one well-defined state where the redox tag moves around due to thermal energy in the other state.

3.1. Sensor characterization and optimization

To study the formation of each sensing probe/layer, cyclic voltammetry (CV) was used to characterize surface assembly by monitoring the electron transfer behavior. As shown in Fig. 2B, voltammograms were

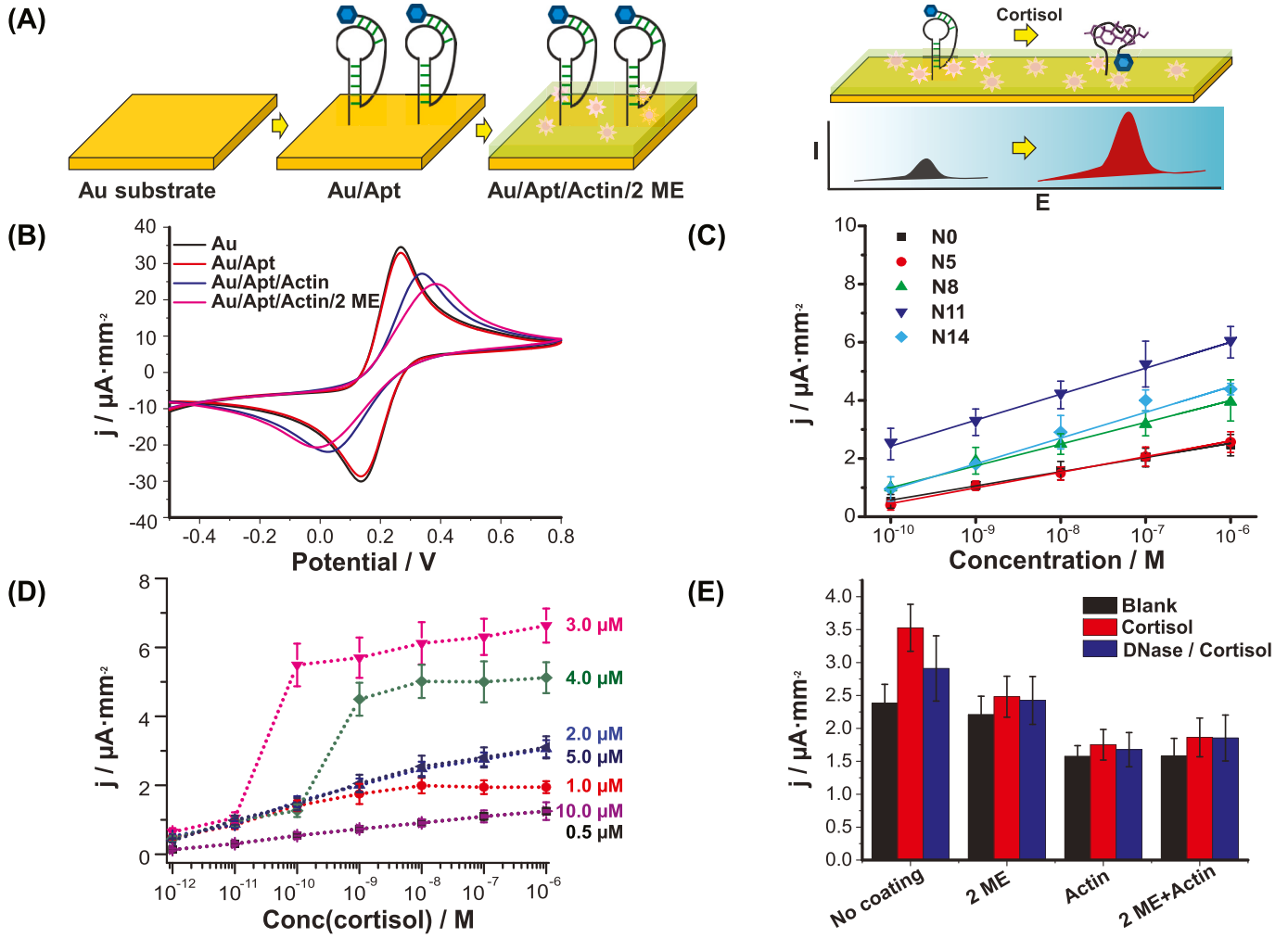

Fig. 2. Sensor characterization and optimization. **(A)** Illustration of sensor fabrication steps and detection principle. **(B)** Stepwise voltammograms of the sensor fabrication in 5 mM $[Fe(CN_6)]^{3-/4-}$ in 1 × PBS. **(C)** Effect of the pseudoknot complementary strand length (N5, N8, N11, N14, where *N* is the number of oligomers and conserved Poly-T_{12} linker in all the structures). **(D)** Aptamer (with pseudoknot-N8) density optimization. **(E)** Effect of surface assembled monolayer (SAM) modification on aptamer stability in the presence of DNase and sensor current response for blank (only 1 × PBS), cortisol (10 nM cortisol spiked in 1 × PBS), and DNase (DNase enzyme at a concentration of 6.5 μU with 30 min incubation time at RT, followed by cortisol). All DPV measurements **(B–E)** were performed in 1 × PBS with a 5 min incubation.

recorded in buffer with ferricyanide from −0.5 to 0.8 V (at a scan rate of 50 mV/s). The bare electrode exhibited well-defined, classic Fe $(CN)_6^{3-/4-}$ redox peaks at +159 and +242 mV, respectively. After aptamer immobilization, the peak current decreased. Further modification of the sensor surface with actin/2 ME led to an increase in the difference between oxidation and reduction potential (ΔE_p) and a significant reduction in the redox current, attributed to the electrode surface passivation with non-conducting moieties (actin/2 ME). These data demonstrated that the sensor was well-formed and able to detect cortisol.

The length of the hybridization region significantly affects the stability of the pseudoknot structure (Hu et al., 2014; Singh et al., 2021c), which in turn leads to a differential current response. In addition, the aptamer density can also affect the sensor performance (Singh et al., 2021a). Hence to achieve maximum sensitivity and minimum variability, optimization experiments were performed. First, the length of the hybridization region was varied ($N = 5$, 8, 11, and 14 bp) to monitor the sensor response. As depicted in Fig. 2C, the N8 aptamer has the least variability while maintaining moderate sensitivity. The N11 and N14 aptamers showed higher sensitivity but suffered from high variability. Likewise, the N5 aptamer exhibited a similar response to the original aptamer (without the pseudoknot). Based on these data, the N8 pseudoknot aptamer was selected for all further studies. Next, the aptamer density was studied as it plays a crucial role in sensor performance. Loosely packed aptamers significantly reduce the signal, particularly in redox-tagged conformation-switching aptasensors, whereas densely packed aptamers can cause steric hindrance restricting conformation changes. The effect of aptamer incubation concentration from 0.5 to 10 μM was examined (Fig. 2D), where 2 μM showed the best linear response over a very broad cortisol concentration range. Concentrations above 2 μM had significant nonlinearities.

Surface blocking with a suitable blocking agent is a well-known process to prevent non-specific adsorption at the sensor surface, which is especially important in wearable and implantable sensors (Singh et al., 2021c; Yasuda et al., 2005, 1996) since they remain in contact with biofluids for a much longer duration than an *in vitro* sensor (Windmiller and Wang, 2013). This prolonged exposure also complicates probe stability, particularly the need for probe (aptamer/protein) protection from nucleases/proteases in biofluids (Shaver et al., 2021). Human sweat contains DNase-I at a very low concentration (6.5 μU/mg) compared to other biofluids (serum, blood, urine, etc.), but can still degrade DNA with long exposure (Baker, 2019; Patterson et al., 2000). Actin and 2 ME are well-known inhibitors of DNase-I activity and are often used as a surface blocking agent (Humpolicek et al., 2012; Robergs

et al., 2004). Thus, the sensor performance was evaluated using these blocking agents and tested in the presence of DNase-I. As shown in Fig. 2E, the maximum response (in the presence of cortisol) and protection (from DNase-I) were simultaneously observed with 2 ME without significantly hampering the electron transfer process. Although a lower signal was observed when adding actin and 2 ME+actin; the 2 ME+actin condition was selected for all further studies to ensure long-term protection of the aptamer from DNase. The protection of DNA from DNase-I was also evaluated with gel electrophoresis, and a similar result was observed (Supplemental Fig. S3).

3.2. pH sensor and microfluidics

Various factors alter the pH of human sweat, such as exercise, drugs, food, and disease (Baker, 2019; Patterson et al., 2000; Robergs et al., 2004). Under normal circumstances, sweat pH varies by one unit from the 6.3 nominal value (Baker, 2019). We fabricated a pH sensor with PANI/Nafion, as both are proven biocompatible materials and have excellent surface sensitivity and selectivity to protonation. The protonation and ion transfer of these electro-active materials strongly depend on the PANI oxidation state and the solution pH (Yokus et al., 2020). The sensor performance was evaluated in buffer solution of various pHs (Supplemental Fig. S4A) after calibration with standard pH (4, 7, and 10) reference solutions. Protonation and deprotonation of PANI at lower or higher pH led to a change in the OCP. The measured sensitivity was 69 ± 8.25 mV/pH. Since the electrochemical behavior of MB and the aptamer binding affinity are pH-dependent (Belleperche and DeRosa, 2018; Ju et al., 1995), the assay performance was evaluated at various pHs (Supplemental Fig. S4B). We observed modulation of the aptasensor performance at acidic pH with the lowest response at pH 5 attributed to poor aptamer conformation switching and binding affinity.

The wearable microfluidic sweat sensor comprises lithographically defined Au electrodes inside microfluidic channels. The flexible microfluidics were prepared using PDMS with 3D printed micro-structured mold, as shown in Fig. 3A. The microfluidic structure was released from the mold by removing the sacrificial PMMA layer using acetone and isopropanol (Fig. 3B). The microfluids are designed to work in a wearable format; thus, physical integrity analysis is essential to ensure smooth operability on the skin. Several permutations of mechanical strain and bending were examined. The microfluidic device showed excellent mechanical stability without any deformity under repeated cycles of bending and stretching using physiologically relevant

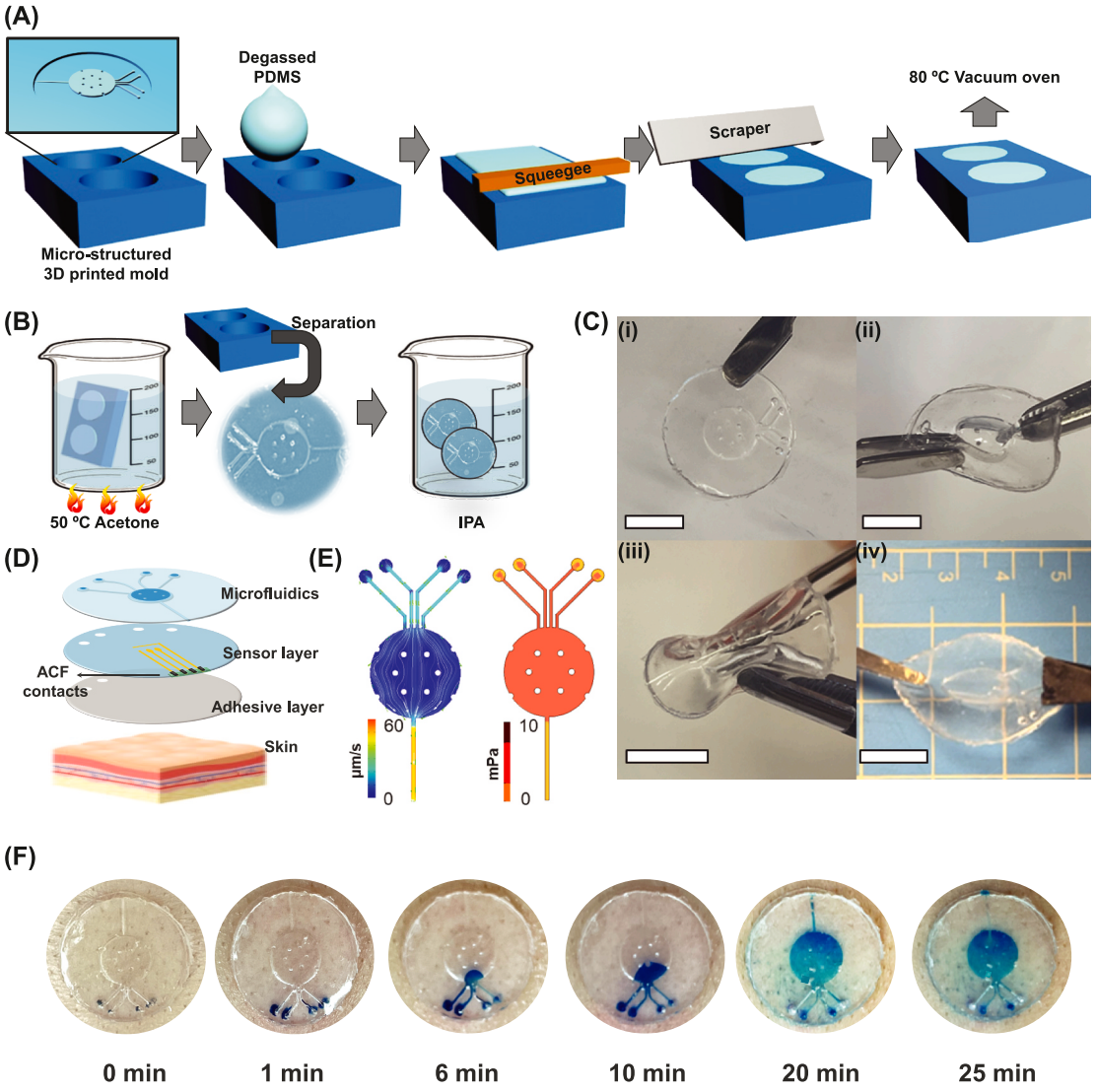

Fig. 3. Fabrication and characterization of microfluidics. (A–B) PDMS microfluidic fabrication process using a 3D printed mold. **(C)** Physical integrity analysis of microfluidic (i) before, (ii) twisting, (iii) bending, and (iv) 25% stretching *in vitro*. Scale bar is 10 mm. **(D)** Microfluidic cross-section diagram. **(E)** Simulation showing sweat velocity and pressure contour in microfluidic channels. **(F)** Photographs of sweat-filling on-body without electrodes at several time points.

conditions (Fig. 3C). The preserved physical integrity enables on-body continuous sweat cortisol monitoring without concern for functional loss during operation. The compact device consists of three flexible layers (20 mm diameter, 1.1 mm thickness), posing structural adaptability with the skin. The device has a medical-grade double-sided adhesive bottom layer with four 2 mm diameter openings for sweat transfer to the middle layer, as shown in Fig. 3D. The middle layer (0.5 mm thickness) is integrated with flexible electrodes and microfluidic vias aligned with the inlets. The topmost layer (0.5 mm thickness) contains microfluidic channels (200 μm height × 200 μm width × 5 mm length) connected to a circular reservoir (7 mm diameter) with an outlet. The layers are sealed by curing the PDMS.

Skin naturally acts as a pump with continuous sweat secretion from sweat glands. Thus, simply adhering the device to skin captures the sweat through the inlets, transfers it through the channels to the detection reservoir over the sensor surface, and expels it into the outlet. Some sweat pores in contact with the adhesive were blocked and influenced the flow rate. However, the sweat pores located within the 2 mm diameter openings of the adhesive layer naturally pump generated sweat through the microfluidic device due to the short distance between the inlet and the sweat pore. The outlet channel dimensions were optimized (6.5 mm length, 0.3 mm width, and 0.2 mm thickness) to ensure that the old sweat was replaced with the new sweat due to the hydrodynamic pressure imposed by the four-inlet configuration. This optimization was done through simulation to verify the flow under standard operating conditions (Fig. 3E). The sweat flows in a streamlined fashion at an inlet velocity of 250.3 nL/min (Francis et al., 2018). The outlet condition was set to zero-gauge pressure. The flow rate and pressure are reduced to sub μm/s at 5 mPa pressure in the reservoir, providing favorable conditions for target-aptamer interaction. Since the outlet pressure is low relative to the inlet and reservoir, pressure gradients are formed, resulting in an increase in the flow rate at the outlet channel to support the replacement of old sweat with new sweat in the reservoir. The time required to fill the detection reservoir should be low to support real-time monitoring and measure temporal modulation in sweat cortisol levels. Thus, the required time to fill the reservoir (on-body and *in vitro* test) was evaluated at 20 μL/min flow rate from one inlet channel to mimic a low sweat rate (Fig. 3F and Supplemental Fig. S5). It required around 60 s to fill the entire device *in vitro*; however, this time increased to 20 min on-body, possibly because of differences in individual's sweat rate.

3.3. *in vitro* electrochemical measurements

The analytical performance of the pseudoknot-assisted aptasensor was evaluated using voltammetry in an *in vitro* setup with and without the microfluidic channels (Fig. 4). The presence of cortisol induced target-dependent aptamer conformation switching, opening the MB-tagged pseudoknot structure. The sensor response was measured in buffer and artificial sweat spiked with cortisol. The sensor displayed a well-defined voltammogram with a clear MB peak between −0.1 and −0.25 V. The observed peak shift between buffer and sweat samples is attributed to the different solution pHs and compositions (Ju et al., 1995). The sensor performance without a microfluidic channel showed an increase in current with increasing cortisol concentration (inset of Fig. 4A,C), indicating successful cortisol binding and unfolding of the pseudoknot structure. A broad linear range from 1 pM to 1 μM with good linearity ($R^2 \geq 0.98$) in buffer and artificial sweat was observed, covering the physiological range of cortisol (21–387 nM) in humans (Russell et al., 2014). The calculated limit of detection (LOD) is 0.17 and 0.2 pM in buffer and artificial sweat, respectively. The sensitivity is 0.33 (μA/mm^2)/cortisol [pM] and 0.24 (μA/mm^2)/cortisol [pM] in buffer and artificial sweat, respectively. The sensor's real-time measurement ability was also evaluated with chronoamperometry at −0.25 V (Supplemental Fig. S6). The sensor responded to increasing cortisol concentration from 0.1 nM to 1 μM in buffer with distinct chronoamperograms. A control experiment without cortisol was also conducted using similar conditions, and no such signal was observed.

With the integrated microfluidic sensor, contrived buffer and artificial sweat sample were pumped at 20 μL/min with gradually increasing cortisol concentration from 1 pM to 1 μM. The measured voltammograms have a distinct peak that increases in response to the cortisol concentration (inset Fig. 4B,D). Calibration plots were generated by plotting the cortisol concentration in buffer (Fig. 4B) and artificial sweat

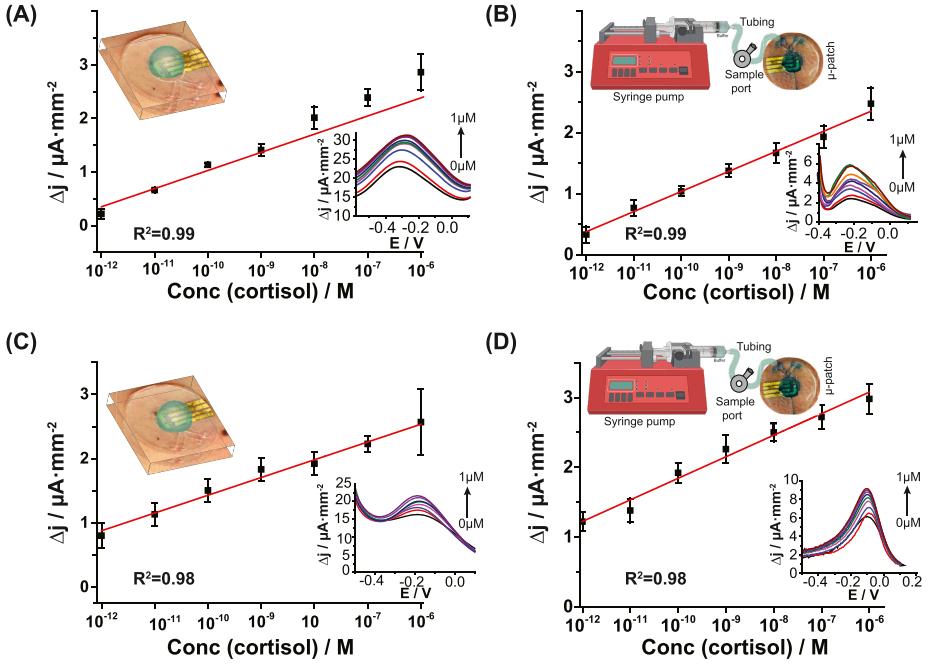

Fig. 4. *in vitro* cortisol measurement. Cortisol was measured in **(A)** buffer without microfluidics, **(B)** buffer with microfluidics, **(C)** artificial sweat without microfluidics, and **(D)** artificial sweat with microfluidics. For all conditions, cortisol was spiked in solution (binding buffer or artificial sweat) at a concentration from 1 pM to 1 μM and measured. All regression lines have $R^2 > 0.98$.

(Fig. 4D) against the observed signal. The sensor had a broad linear range, like the case without the microfluidics. The measured LOD is 1.35 pM and 1.56 pM in buffer and artificial sweat, respectively. The sensitivity is 0.25 (μA/mm^2)/cortisol [pM] in buffer and 0.31(μA/mm^2)/cortisol [pM] in artificial sweat. Overall, the sensor is very sensitive and has a rapid response in the presence of cortisol. These data demonstrate the high performance of the pseudoknot-assisted aptasensor with integrated microfluidics covering the physiological cortisol concentration range.

3.4. Sensor performance

A wearable sensor will be sensitive to variation in skin temperature, as the aptamer binding affinity and MB activation energy are directly influenced by the temperature (Hasegawa et al., 2016; Saeed, 2014). Thus, the sensor performance was evaluated at various temperatures ranging from 25 to 35 °C (Fig. 5A). The sensor exhibited 30% higher sensitivity at 35 °C compared to 25 °C, which we attribute to the lowering of the MB activation energy. Thus, calibration at various temperatures is required to maintain sensor accuracy. It is crucial to have crosstalk-free operation in the presence of potentially interfering constituents of sweat, such as glucose, epinephrine, ascorbic acid, IgG, and CRP. Having already shown cortisol detection in artificial sweat, these potential interferents were spiked in buffer at their basal level in human sweat and measured using similar conditions (Fig. 5B). The signal was 4–10 × higher for cortisol than the interferent in each case. These data demonstrate the specificity of the pseudoknot-assisted aptamer. Finally, sensor regeneration is a prerequisite for wearable sensing applications. We performed regeneration measurements where the sensor was successfully regenerated 2 × without significant loss in binding affinity and sensor performance (Supplemental Fig. S7).

3.5. in situ on-body sweat measurement

On-body, real-time monitoring of sweat cortisol was performed to evaluate the performance of the sweat patch in practical scenarios from three healthy individuals under induced stress conditions by the cold pressure test (CPT) (Shida et al., 2020) during exercise. The experiments were performed in accordance with an approved UCSD institutional review board protocol. Sweat patches were applied to the lower necks of subjects, as shown in Fig. 6A. The time to fill the sweat patch reservoir with and without an electrode was analyzed. As depicted in Fig. 6B, the blue dye in each inlet began to diffuse at the start of sweat flow (1 min). The flow spread outwardly toward the reservoir (10 min), and after 20 min, the sensing chamber (reservoir) was filled, and sweat started coming out for the constant replacement from the outlet channel within 25 min. Similar fluid dynamics pattern and filling time was observed with and without the electrodes. It is worth noting that temperature, environment, and exercise conditions can alter the sweat rate and, consequently, the reservoir filling time.

Temporal changes in sweat cortisol levels under external stress conditions were monitored for 30 min during indoor cycling from three different subjects (Fig. 6D–F). The three subjects' continuous amperometric sweat cortisol response showed an increase in signal as the sweat filled the reservoirs and completed the circuit, ranging from 6 to 10 min. Compared to the control, a rapid increase in signal was observed in all three subjects after CPT. As expected, after the induced shock (Shida et al., 2020), cortisol levels increased significantly and returned to their basal level (control) after removal from CPT. This real-time profile was different for each subject. This indicates that the observed increase in signal was solely from the aptamer and sweat cortisol interaction and not from other sweat constituents. Compared to *in vitro* tests (Fig. 4D), the signal variation among the subjects suggests that a combination of factors (flow rate, pH, composition, and temperature) also affect the amperometric response. Moreover, the control and test signal variation among the subjects reflects the difference in basal cortisol level and endurance to tolerate stress (Knutsson et al., 1997). While physical activity was used to induce sweating in this work, iontophoresis (electrically driven release of chemicals such as pilocarpine or cevimeline) is also viable – with benefits in a non-performance situation (*e.g.*, a medical wearable). Thus, continuous monitoring of individual cortisol levels will support precision medicine and allow for better treatment (Stone et al., 2001).

We further evaluated the sensor performance under long-term (1.5 h) continuous monitoring with on-body signal regeneration. Briefly, a healthy volunteer was exposed to intermittent induced shock conditions during the exercise (cycling on a stationary exercise bike). As depicted in Fig. 6G, a negligible signal was observed during the initial period of exercise, followed by a rapid increase after sweat fills the reservoir, which subsequently returned to a normal level in 7–8 min. Stress was induced by CPT, causing the cortisol signal to increase significantly and allowed to return to a normal level before again inducing stress. These data demonstrate an on-body sensor's continuous monitoring, regeneration, and aptamer stability of an on-body sensor. Long-term storage of the aptasensor was not explored in this work but has been shown to be robust with minimal performance degradation (Fan and Yang, 2022; Zhen et al., 2020). For accurate quantification, the measurement should be pre- and post-calibrated for temperature- and pH-dependence.

3.6 Performance comparison. This work is compared against state-of-the-art wearable cortisol sensors in Supplemental Table S2. Fernandez et al. reported a sensitive but multistep technique in a point-of-care testing (POCT) format with a narrow linear dynamic range (100 pM–50 nM) using electrochemical reduction over a Cu-PP electrode (Fernandez et al., 2017). Wang et al. reported a field effect transistor with an aptamer (aptaFET) for on-body direct measurement on a flexible polyimide electrode with a very low LOD (1 pM) but with a compromised

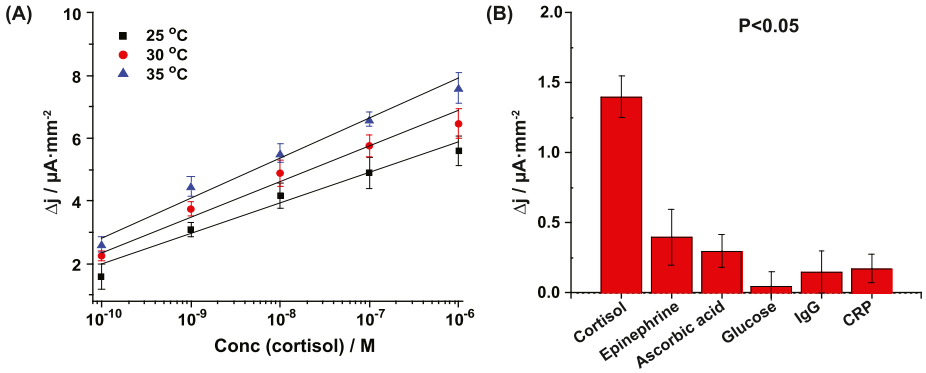

Fig. 5. Sensor performance. (A) Effect of temperature (25, 30, and 35 °C) on the sensor in binding buffer. The regression line has $R^2 > 0.98$ for all curves. **(B)** Measured sensor specificity against potential sweat interferents such as epinephrine (1 μM), ascorbic acid (1 mM), glucose (1 mM), IgG (0.67 nM), and CRP (8.3 pM) spiked in buffer compared against cortisol (10 nM).

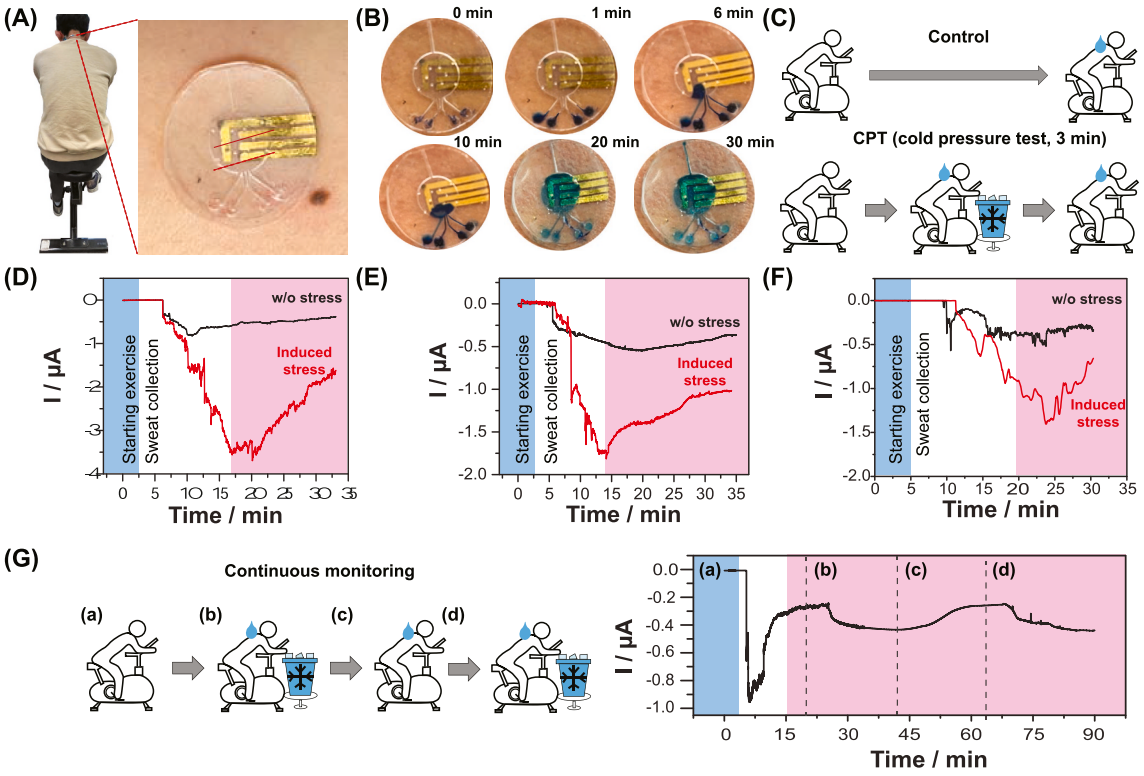

Fig. 6. Real-time on-body amperometric response of sweat cortisol from induced stress using cold pressure test (CPT). (A) Depiction of on-body sweat patch application to the lower neck of the subjects during trials. **(B)** Photographs of sweat filling the microfluidic reservoir during exercise. Blue dye was placed in each inlet before on-body application for visualization. **(C)** Illustration of test protocol (control and induced stress). **(D–F)** Continuous sweat monitoring data from the three different human subjects. **(G)** Long-term continuous monitoring and on-body signal regeneration measurement.

dynamic range (1 pM–1 µM) (B. Wang et al., 2022). An et al. reported a flexible wearable sensor consisting of nanofiber, polyacrylonitrile, and carboxylated poly(3,4-ethylene dioxythiophene) sensor with a liquid ion-gated FET; however, it lacks a suitable mechanism to prevent sweat mixing between the old and new sweat, and thus is not suitable for long-term continuous monitoring (An et al., 2022). Pali et al. developed a "near to wearable sensor" by immobilizing an aptamer on a Zn–O/polyimide patch, and cortisol measurement was performed with electrochemical impedance spectroscopy (Pali et al., 2021). Singh et al. and Mugo et al. developed an electrochemical aptasensor in a POCT format with high performance, but its wearability wasn't demonstrated (Mugo et al., 2021; Singh et al., 2021a). Our approach's key strength and novelty lie in using a pseudoknot aptamer over the DNase-resistant self-assembled monolayer with an integrated microfluidic channel to provide excellent sensitivity and regeneration ability, even under very long-term continuous monitoring on the body. The sweat patch device has the potential to provide pH-calibrated accurate cortisol measurement in real-time from human sweat with reagent-less operation.

4. Conclusion

This study demonstrated a pseudoknot-assisted aptasensor integrated with microfluidics in a wearable format to continuously monitor cortisol in sweat. Modifying an existing aptamer to add a pseudoknot structure enabled highly sensitive detection of cortisol down to sub-pM levels by reducing the background noise due to the disorientation of the MB reporter. Moreover, including a skin-conforming microfluidic channel with multiple sample inlets and a single outlet facilitates rapid filling time for natural sweat sampling and *in-situ* sweat replacement, respectively. The sensor detected cortisol in artificial sweat solutions ranging from 1 pM to 1 µM with an excellent LOD of 0.2 pM and good linearity (R^2 = 0.98). The sensor also exhibited high specificity and reproducibility. This sensor offers the possibility of accurate cortisol quantification in conjunction with sweat pH-calibrated response from an integrated pH sensor in the sweat patch. On-body cortisol monitoring in normal and induced stress conditions with human subjects demonstrates the capabilities of on-body electrochemical monitoring in various sweating conditions with the ability to detect real-time fluctuations in cortisol levels. This new pseudoknot-assisted aptasensor with microfluidic sweat bioelectronic patch can be expanded to the real-time non-invasive monitoring of other sweat biomarkers (*e.g.*, immunoglobulins, CRP, etc.), ushering in a new generation of nearly reagent-less, aptamer-based wearable sensors for continuous monitoring of immune health.

CRediT authorship contribution statement

Naveen K. Singh: Conceptualization, Investigation, Formal analysis, Writing – original draft. **Saeromi Chung:** Conceptualization, Investigation, Formal analysis, Writing – original draft. **An-Yi Chang:** Investigation, Formal analysis. **Joseph Wang:** Conceptualization, Formal analysis, Writing – review & editing, Supervision, Project administration, Funding acquisition. **Drew A. Hall:** Conceptualization, Formal analysis, Writing – review & editing, Supervision, Project administration, Funding acquisition.

Declaration of competing interest

The authors declare that they have no known competing financial interests or personal relationships that could have appeared to influence the work reported in this paper.

Data availability

Data will be made available on request.

Acknowledgments

This work was partly supported by the UCSD Center for Wearable Sensors (CWS). The authors thank Andreas Duvvuri for his help with the sensor nanofabrication.

Appendix A. Supplementary data

Supplementary data to this article can be found online at https://doi.org/10.1016/j.bios.2023.115097.

References

An, J.E., Kim, K.H., Park, S.J., Seo, S.E., Kim, J., Ha, S., Bae, J., Kwon, O.S., 2022. Wearable cortisol aptasensor for simple and rapid real-time monitoring. ACS Sens. 7, 99–108. https://doi.org/10.1021/acssensors.1c01734.

Anastasova, S., Crewther, B., Bembnowicz, P., Curto, V., Ip, H.M., Rosa, B., Yang, G.-Z., 2017. A wearable multisensing patch for continuous sweat monitoring. Biosens. Bioelectron., Special Issue Selected papers from the 26th Anniversary World Congress on Biosensors (Part II) 93, 139–145. https://doi.org/10.1016/j.bios.2016.09.038.

Baker, L.B., 2019. Physiology of sweat gland function: the roles of sweating and sweat composition in human health. Temp. Multidiscip. Biomed. J. 6, 211–259. https://doi.org/10.1080/23328940.2019.1632145.

Bandodkar, A.J., Jeerapan, I., You, J.-M., Nuñez-Flores, R., Wang, J., 2016. Highly stretchable fully-printed CNT-based electrochemical sensors and biofuel cells: combining intrinsic and design-induced stretchability. Nano Lett. 16, 721–727. https://doi.org/10.1021/acs.nanolett.5b04549.

Belleperche, M., DeRosa, M.C., 2018. pH-control in aptamer-based diagnostics, therapeutics, and analytical applications. Pharmaceuticals 11, 80. https://doi.org/10.3390/ph11030080.

Brasier, N., Eckstein, J., 2019. Sweat as a source of next-generation digital biomarkers. Digit. Biomark. 3, 155–165. https://doi.org/10.1159/000504387.

Brunetti B, D.E., 2015. About estimating the limit of detection by the signal to noise approach. Pharm. Anal. Acta. https://doi.org/10.4172/2153-2435.1000355, 06.

Chen, J., Tang, J., Meng, H.-M., Liu, Z., Wang, L., Geng, X., Wu, Y., Qu, L., Li, Z., 2020. Recognition triggered assembly of split aptamers to initiate a hybridization chain reaction for wash-free and amplified detection of exosomes. Chem. Commun. Camb. Engl. 56, 9024–9027. https://doi.org/10.1039/d0cc02337j.

Chrousos, G.P., 2009. Stress and disorders of the stress system. Nat. Rev. Endocrinol. 5, 374–381. https://doi.org/10.1038/nrendo.2009.106.

Chung, S., Sicklick, J.K., Ray, P., Hall, D.A., 2021. Development of a soluble KIT electrochemical aptasensor for cancer theranostics. ACS Sens. 9.

Dang, W., Manjakkal, L., Navaraj, W.T., Lorenzelli, L., Vinciguerra, V., Dahiya, R., 2018. Stretchable wireless system for sweat pH monitoring. Biosens. Bioelectron. 107, 192–202. https://doi.org/10.1016/j.bios.2018.02.025.

De Giovanni, N., Fucci, N., 2013. The current status of sweat testing for drugs of abuse: a review. Curr. Med. Chem. 20, 545–561. https://doi.org/10.2174/0929867311320040006.

Drolen, C., Conklin, E., Hetterich, S.J., Krishnamurthy, A., Andrade, G.A., Dimeglio, J.L., Martin, M.I., Tran, L.K., Yap, G.P.A., Rosenthal, J., Young, E.R., 2018. pH-driven mechanistic switching from electron transfer to energy transfer between [Ru(bpy)3]2+ and ferrocene derivatives. J. Am. Chem. Soc. 140, 10169–10178. https://doi.org/10.1021/jacs.8b03933.

Etiwy, M., Akhrass, Z., Gillinov, L., Alashi, A., Wang, R., Blackburn, G., Gillinov, S.M., Phelan, D., Gillinov, A.M., Houghtaling, P.L., Javadikasgari, H., Desai, M.Y., 2019. Accuracy of wearable heart rate monitors in cardiac rehabilitation. Cardiovasc. Diagn. Ther. 9, 262–271. https://doi.org/10.21037/cdt.2019.04.08.

Fan, J., Yang, W., 2022. Electrochemical DNA/aptamer biosensors based on SPAAC for detection of DNA and protein. Sensor. Actuator. B Chem. 353, 131100 https://doi.org/10.1016/j.snb.2021.131100.

Ferguson, B.S., Hoggarth, D.A., Maliniak, D., Ploense, K., White, R.J., Woodward, N., Hsieh, K., Bonham, A.J., Eisenstein, M., Kippin, T.E., Plaxco, K.W., Soh, H.T., 2013. Real-time, aptamer-based tracking of circulating therapeutic agents in living animals. Sci. Transl. Med. 5 https://doi.org/10.1126/scitranslmed.3007095, 213ra165-213ra165.

Fernandez, R.E., Umasankar, Y., Manickam, P., Nickel, J.C., Iwasaki, L.R., Kawamoto, B. K., Todoki, K.C., Scott, J.M., Bhansali, S., 2017. Disposable aptamer-sensor aided by magnetic nanoparticle enrichment for detection of salivary cortisol variations in obstructive sleep apnea patients. Sci. Rep. 7, 17992 https://doi.org/10.1038/s41598-017-17835-8.

Francis, J., Stamper, I., Heikenfeld, J., Gomez, E.F., 2018. Digital nanoliter to milliliter flow rate sensor with in vivo demonstration for continuous sweat rate measurement. Lab Chip 19, 178–185. https://doi.org/10.1039/C8LC00968F.

Gao, W., Emaminejad, S., Nyein, H.Y.Y., Challa, S., Chen, K., Peck, A., Fahad, H.M., Ota, H., Shiraki, H., Kiriya, D., Lien, D.-H., Brooks, G.A., Davis, R.W., Javey, A., 2016. Fully integrated wearable sensor arrays for multiplexed in situ perspiration analysis. Nature 529, 509–514. https://doi.org/10.1038/nature16521.

Ghaffari, R., Yang, D.S., Kim, J., Mansour, A., Wright, J.A., Model, J.B., Wright, D.E., Rogers, J.A., Ray, T.R., 2021. State of sweat: emerging wearable systems for real-time, noninvasive sweat sensing and analytics. ACS Sens. 6, 2787–2801. https://doi.org/10.1021/acssensors.1c01133.

Gordon, C.K.L., Eisenstein, M., Soh, H.T., 2018. Direct selection strategy for isolating aptamers with pH-sensitive binding activity. ACS Sens. 3, 2574–2580. https://doi.org/10.1021/acssensors.8b00945.

Hasegawa, H., Savory, N., Abe, K., Ikebukuro, K., 2016. Methods for improving aptamer binding affinity. Mol. Basel Switz. 21, 421. https://doi.org/10.3390/molecules21040421.

Heikenfeld, J., 2016. Non-invasive analyte access and sensing through eccrine sweat: challenges and outlook circa 2016. Electroanalysis 28, 1242–1249. https://doi.org/10.1002/elan.201600018.

Herrmann, F., Mandol, L., 1955. Studies of ph of sweat produced by different forms of stimulation. J. Invest. Dermatol. 24, 225–246. https://doi.org/10.1038/jid.1955.36.

Hu, R., Liu, T., Zhang, X.-B., Huan, S.-Y., Wu, C., Fu, T., Tan, W., 2014. Multicolor fluorescent biosensor for multiplexed detection of DNA. Anal. Chem. 86, 5009–5016. https://doi.org/10.1021/ac500618v.

huber, zak, 2016. Continuous Glucose Monitoring (CGM) | 24 Hour Glucose Monitor [WWW Document]. Dexcom. URL. https://www.dexcom.com/continuous-glucose-monitoring, 3.30.22.

Humpolicek, P., Kasparkova, V., Saha, P., Stejskal, J., 2012. Biocompatibility of polyaniline. Synth. Met. 162, 722–727. https://doi.org/10.1016/j.synthmet.2012.02.024.

Jiang, B., Li, F., Yang, C., Xie, J., Xiang, Y., Yuan, R., 2015. Aptamer pseudoknot-functionalized electronic sensor for reagentless and single-step detection of immunoglobulin E in human serum. Anal. Chem. 87, 3094–3098. https://doi.org/10.1021/acs.analchem.5b00041.

Ju, H., Zhou, J., Cai, C., Chen, H., 1995. The electrochemical behavior of methylene blue at a microcylinder carbon fiber electrode. Electroanalysis 7, 1165–1170. https://doi.org/10.1002/elan.1140071213.

Katchman, B.A., Zhu, M., Christen, J.B., Anderson, K.S., 2018. Eccrine sweat as a biofluid for profiling immune biomarkers. PROTEOMICS – clin. Apple 12, 1800010. https://doi.org/10.1002/prca.201800010.

Kim, J., Jeerapan, I., Imani, S., Cho, T.N., Bandodkar, A., Cinti, S., Mercier, P.P., Wang, J., 2016. Noninvasive alcohol monitoring using a wearable tattoo-based iontophoretic-biosensing system. ACS Sens. 1, 1011–1019. https://doi.org/10.1021/acssensors.6b00356.

Kinnamon, D., Ghanta, R., Lin, K.-C., Muthukumar, S., Prasad, S., 2017. Portable biosensor for monitoring cortisol in low-volume perspired human sweat. Sci. Rep. 7, 13312 https://doi.org/10.1038/s41598-017-13684-7.

Kintz, P., Tracqui, A., Mangin, P., Edel, Y., 1996. Sweat testing in opioid users with a sweat patch. J. Anal. Toxicol. 20, 393–397. https://doi.org/10.1093/jat/20.6.393.

Knutsson, U., Dahlgren, J., Marcus, C., Rosberg, S., Brönnegård, M., Stierna, P., Albertsson-Wikland, K., 1997. Circadian cortisol rhythms in healthy boys and girls: relationship with age, growth, body composition, and pubertal development. J. Clin. Endocrinol. Metab. 82, 536–540. https://doi.org/10.1210/jcem.82.2.3769.

Koh, A., Kang, D., Xue, Y., Lee, S., Pielak, R.M., Kim, J., Hwang, T., Min, S., Banks, A., Bastien, P., Manco, M.C., Wang, L., Ammann, K.R., Jang, K.-I., Won, P., Han, S., Ghaffari, R., Paik, U., Slepian, M.J., Balooch, G., Huang, Y., Rogers, J.A., 2016. A soft, wearable microfluidic device for the capture, storage, and colorimetric sensing of sweat. Sci. Transl. Med. 8 https://doi.org/10.1126/scitranslmed.aaf2593, 366ra165-366ra165.

Mahmud, M.S., Fang, H., Wang, H., Carreiro, S., Boyer, E., 2018. Automatic detection of opioid intake using wearable biosensor. In: Int. Conf. Comput. Netw. Commun. Proc. Int. Conf. Comput. Netw. Commun., pp. 784–788. https://doi.org/10.1109/ICCNC.2018.8390334, 2018.

Martín, A., Kim, J., Kurniawan, J.F., Sempionatto, J.R., Moreto, J.R., Tang, G., Campbell, A.S., Shin, A., Lee, M.Y., Liu, X., Wang, J., 2017. Epidermal microfluidic electrochemical detection system: enhanced sweat sampling and metabolite detection. ACS Sens. 2, 1860–1868. https://doi.org/10.1021/acssensors.7b00729.

Mugo, S.M., Alberkant, J., Bernstein, N., Zenkina, O.V., 2021. Flexible electrochemical aptasensor for cortisol detection in human sweat. Anal. Methods 13, 4169–4173. https://doi.org/10.1039/D1AY01233A.

Nyein, H.Y.Y., Tai, L.-C., Ngo, Q.P., Chao, M., Zhang, G.B., Gao, W., Bariya, M., Bullock, J., Kim, H., Fahad, H.M., Javey, A., 2018. A wearable microfluidic sensing patch for dynamic sweat secretion analysis. ACS Sens. 3, 944–952. https://doi.org/10.1021/acssensors.7b00961.

Oncescu, V., O'Dell, D., Erickson, D., 2013. Smartphone based health accessory for colorimetric detection of biomarkers in sweat and saliva. Lab Chip 13, 3232–3238. https://doi.org/10.1039/c3lc50431j.

Pali, M., Jagannath, B., Lin, K.-C., Upasham, S., Sankhalab, D., Upashama, S., Muthukumar, S., Prasad, S., 2021. CATCH (cortisol apta WATCH): 'bio-mimic alarm' to track anxiety, stress, immunity in human sweat. Electrochim. Acta 390, 138834. https://doi.org/10.1016/j.electacta.2021.138834.

Parlak, O., Keene, S.T., Marais, A., Curto, V.F., Salleo, A., 2018. Molecularly selective nanoporous membrane-based wearable organic electrochemical device for noninvasive cortisol sensing. Sci. Adv. 4, eaar2904 https://doi.org/10.1126/sciadv.aar2904.

Patel, S., Park, H., Bonato, P., Chan, L., Rodgers, M., 2012. A review of wearable sensors and systems with application in rehabilitation. J. NeuroEng. Rehabil. 9, 21. https://doi.org/10.1186/1743-0003-9-21.

Patterson, M.J., Galloway, S.D., Nimmo, M.A., 2000. Variations in regional sweat composition in normal human males. Exp. Physiol. 85, 869–875. https://doi.org/10.1111/j.1469-445x.2000.02058.x.

Plaxco, K.W., Soh, H.T., 2011. Switch-based biosensors: a new approach towards real-time, in vivo molecular detection. Trends Biotechnol. 29, 1–5. https://doi.org/10.1016/j.tibtech.2010.10.005.

Robergs, R.A., Ghiasvand, F., Parker, D., 2004. Biochemistry of exercise-induced metabolic acidosis. Am. J. Physiol. Regul. Integr. Comp. Physiol. 287, R502–R516. https://doi.org/10.1152/ajpregu.00114.2004.

Russell, E., Koren, G., Rieder, M., Van Uum, S.H.M., 2014. The detection of cortisol in human sweat: implications for measurement of cortisol in hair. Ther. Drug Monit. 36, 30–34. https://doi.org/10.1097/FTD.0b013e31829daa0a.

Saeed, R.S., 2014. The kinetics of electron transfer reaction of methylene blue and titanium trichloride in different solvents. J. Adv. Chem. 6, 940–957. https://doi.org/10.24297/jac.v6i2.6583.

Sakihara, S., Kageyama, K., Oki, Y., Doi, M., Iwasaki, Y., Takayasu, S., Moriyama, T., Terui, K., Nigawara, T., Hirata, Y., Hashimoto, K., Suda, T., 2010. Evaluation of plasma, salivary, and urinary cortisol levels for diagnosis of cushing's syndrome. Endocr. J. 57, 331–337. https://doi.org/10.1507/endocrj.K09E-340.

Samson, C., Koh, A., 2020. Stress monitoring and recent advancements in wearable biosensors. Front. Bioeng. Biotechnol. 8.

Sanjay, M., Singh, N.K., Ngashangva, L., Goswami, P., 2020. A smartphone-based fiber-optic aptasensor for label-free detection of Plasmodium falciparum glutamate dehydrogenase. Anal. Methods 12, 1333–1341. https://doi.org/10.1039/C9AY02406A.

Schoukroun-Barnes, L.R., Macazo, F.C., Gutierrez, B., Lottermoser, J., Liu, J., White, R.J., 2016. Reagentless, structure-switching, electrochemical aptamer-based sensors. Annu. Rev. Anal. Chem. 9, 163–181. https://doi.org/10.1146/annurev-anchem-071015-041446.

Sempionatto, J.R., Nakagawa, T., Pavinatto, A., Mensah, S.T., Imani, S., Mercier, P., Wang, J., 2017. Eyeglasses based wireless electrolyte and metabolite sensor platform. Lab Chip 17, 1834–1842. https://doi.org/10.1039/c7lc00192d.

Shaver, A., Kundu, N., Young, B.E., Vieira, P.A., Sczepanski, J.T., Arroyo-Currás, N., 2021. Nuclease hydrolysis does not drive the rapid signaling decay of DNA aptamer-based electrochemical sensors in biological fluids. Langmuir 37, 5213–5221. https://doi.org/10.1021/acs.langmuir.1c00166.

Shida, A., Ikeda, T., Tani, N., Morioka, F., Aoki, Y., Ikeda, K., Watanabe, M., Ishikawa, T., 2020. Cortisol levels after cold exposure are independent of adrenocorticotropic hormone stimulation. PLoS One 15, e0218910. https://doi.org/10.1371/journal.pone.0218910.

Singh, N.K., Jain, P., Das, S., Goswami, P., 2019. Dye coupled aptamer-captured enzyme catalyzed reaction for detection of Pan malaria and P. Falciparum species in laboratory settings and instrument-free paper-based platform. Anal. Chem. 91, 4213–4221. https://doi.org/10.1021/acs.analchem.9b00670.

Singh, N.K., Chung, S., Sveiven, M., Hall, D.A., 2021a. Cortisol detection in undiluted human serum using a sensitive electrochemical structure-switching aptamer over an antifouling nanocomposite layer. ACS Omega 6, 27888–27897. https://doi.org/10.1021/acsomega.1c03552.

Singh, N.K., Ray, P., Carlin, A.F., Magallanes, C., Morgan, S.C., Laurent, L.C., Aronoff-Spencer, E.S., Hall, D.A., 2021b. Hitting the diagnostic sweet spot: point-of-care SARS-CoV-2 salivary antigen testing with an off-the-shelf glucometer. Biosens. Bioelectron. 113111 https://doi.org/10.1016/j.bios.2021.113111.

Singh, N.K., Ray, P., Carlin, A.F., Morgan, S.C., Magallanes, C., Laurent, L.C., Aronoff-Spencer, E.S., Hall, D.A., 2021c. Dataset on optimization and development of a point-of-care glucometer-based SARS-CoV-2 detection assay using aptamers. Data Brief 38, 107278. https://doi.org/10.1016/j.dib.2021.107278.

Stone, A.A., Schwartz, J.E., Smyth, J., Kirschbaum, C., Cohen, S., Hellhammer, D., Grossman, S., 2001. Individual differences in the diurnal cycle of salivary free cortisol: a replication of flattened cycles for some individuals. Psychoneuroendocrinology 26, 295–306. https://doi.org/10.1016/s0306-4530(00)00057-3.

Vinoth, R., Nakagawa, T., Mathiyarasu, J., Mohan, A.M.V., 2021. Fully printed wearable microfluidic devices for high-throughput sweat sampling and multiplexed electrochemical analysis. ACS Sens. 6, 1174–1186. https://doi.org/10.1021/acssensors.0c02446.

Wang, B., Zhao, C., Wang, Z., Yang, K.-A., Cheng, X., Liu, W., Yu, W., Lin, S., Zhao, Y., Cheung, K.M., Lin, H., Hojaiji, H., Weiss, P.S., Stojanović, M.N., Tomiyama, A.J., Andrews, A.M., Emaminejad, S., 2022. Wearable aptamer-field-effect transistor sensing system for noninvasive cortisol monitoring. Sci. Adv. 8, eabk0967 https://doi.org/10.1126/sciadv.abk0967.

Wang, M., Yang, Y., Min, J., Song, Y., Tu, J., Mukasa, D., Ye, C., Xu, C., Heflin, N., McCune, J.S., Hsiai, T.K., Li, Z., Gao, W., 2022. A wearable electrochemical biosensor for the monitoring of metabolites and nutrients. Nat. Biomed. Eng. 6, 1225–1235. https://doi.org/10.1038/s41551-022-00916-z.

Windmiller, J.R., Wang, J., 2013. Wearable electrochemical sensors and biosensors: a review. Electroanalysis 25, 29–46. https://doi.org/10.1002/elan.201200349.

Wu, H., Huang, B., Zare, R.N., 2005. Construction of microfluidic chips using polydimethylsiloxane for adhesive bonding. Lab Chip 5, 1393–1398. https://doi.org/10.1039/B510494G.

Xu, S., Zhang, Y., Jia, L., Mathewson, K.E., Jang, K.-I., Kim, J., Fu, H., Huang, X., Chava, P., Wang, R., Bhole, S., Wang, L., Na, Y.J., Guan, Y., Flavin, M., Han, Z., Huang, Y., Rogers, J.A., 2014. Soft microfluidic assemblies of sensors, circuits, and radios for the skin. Science 344, 70–74. https://doi.org/10.1126/science.1250169.

Yang, K.-A., Chun, H., Zhang, Y., Pecic, S., Nakatsuka, N., Andrews, A.M., Worgall, T.S., Stojanovic, M.N., 2017. High-affinity nucleic-acid-based receptors for steroids. ACS Chem. Biol. 12, 3103–3112. https://doi.org/10.1021/acschembio.7b00634.

Yasuda, T., Takeshita, H., Sawazaki, K., Iida, R., Kishi, K., 1996. Successful deoxyribonuclease I (DNase I) phenotyping from a small piece of used sock. Electrophoresis 17, 1253–1256. https://doi.org/10.1002/elps.1150170714.

Yasuda, T., Kawai, Y., Ueki, M., Kishi, K., 2005. Clinical applications of DNase I, a genetic marker already used for forensic identification. Leg. Med. 7, 274–277. https://doi.org/10.1016/j.legalmed.2004.10.008.

Yokus, M.A., Songkakul, T., Pozdin, V.A., Bozkurt, A., Daniele, M.A., 2020. Wearable multiplexed biosensor system toward continuous monitoring of metabolites. Biosens. Bioelectron. 153, 112038 https://doi.org/10.1016/j.bios.2020.112038.

Zeng, X., Peng, R., Fan, Z., Lin, Y., 2022. Self-powered and wearable biosensors for healthcare. Mater. Today Energy 23, 100900. https://doi.org/10.1016/j.mtener.2021.100900.

Zhen, J., Liang, G., Chen, R., Jia, W., 2020. Label-free hairpin-like aptamer and EIS-based practical, biostable sensor for acetamiprid detection. PLoS One 15, e0244297. https://doi.org/10.1371/journal.pone.0244297.